Matter-wave solitons in radially periodic potentials

Bakhtiyor B. Baizakov,[1] Boris A. Malomed,[2] and Mario Salerno[3]
[1]*Physical-Technical Institute of the Uzbek Academy of Sciences, 2-b, G. Mavlyanov Strasse, 700084, Tashkent, Uzbekistan*
[2]*Department of Interdisciplinary Studies, School of Electrical Engineering, Faculty of Engineering, Tel Aviv University, Tel Aviv 69978, Israel*
[3]*Dipartimento di Fisica "E. R. Caianiello," Consorzio Nazionale Interuniversitario per le Scienze Fisiche della Materia (CNISM), Universitá di Salerno, I-84081, Baronissi, Salerno, Italy*
(Received 6 May 2006; revised manuscript received 16 August 2006; published 29 December 2006)

We investigate two-dimensional (2D) states in Bose-Einstein condensates with self-attraction or self-repulsion, trapped in an axially symmetric optical-lattice potential periodic along the radius. The states trapped both in the central potential well and in remote circular troughs are studied. In the repulsive mode, a new soliton species is found, in the form of radial gap solitons. The latter solitons are completely stable if they carry zero vorticity ($l=0$), while with $l\neq 0$ they develop a weak azimuthal modulation, which makes them rotating patterns, that persist indefinitely long. In addition, annular gap solitons may support stable azimuthal dark-soliton pairs on their crests. In remote troughs of the attractive model, stable localized states may assume a ringlike shape with weak azimuthal modulation, or shrink into solitons strongly localized in the azimuthal direction, which is explained in the framework of an averaged 1D equation with the cyclic azimuthal coordinate. Numerical simulations of the attractive model also reveal stable necklacelike patterns, built of several strongly localized peaks. Dynamics of strongly localized solitons circulating in the troughs is studied too. While the solitons with sufficiently small velocities are completely stable, fast solitons gradually decay, due to the leakage of matter into the adjacent trough, under the action of the centrifugal force. Investigation of head-on collisions between strongly localized solitons traveling in circular troughs shows that collisions between in-phase solitons in a common trough lead to collapse, while π-out-of-phase solitons bounce many times, but eventually merge into a single one, without collapsing. In-phase solitons colliding in adjacent circular troughs also tend to merge into a single soliton.

DOI: 10.1103/PhysRevE.74.066615 PACS number(s): 42.65.Tg, 03.75.Kk, 42.65.Jx

I. INTRODUCTION

Matter-wave solitons, that can be created in Bose-Einstein condensates (BECs), are a research subject of great interest, both as nonlinear collective excitations in macroscopic quantum matter, and due to the potential they offer in applications to high-precision interferometry, matter-wave lasers, quantum information processing, and other emerging technologies. Dark and bright matter-wave solitons were experimentally created in nearly one-dimensional (1D) traps filled with ^{87}Rb [1] and ^{7}Li [2,3] condensate, respectively. In these settings, strong radial confinement freezes transverse dynamics of the condensate, keeping atoms (with mass m) in the ground state of the corresponding 2D harmonic-oscillator potential $m\omega_{\perp}^2 r^2/2$, while a weak axial parabolic trap $m\omega_{\parallel}^2 x^2/2$ allows quasifree motion of the soliton in the axial direction x. New recent experiments with ^{85}Rb [4] and related numerical simulations [5] have showed the existence of stable solitary waves, supported by attraction between atoms, in a weakly elongated ($\omega_{\perp}/\omega_x \simeq 2.5$) trap. These essentially three-dimensional (3D) bright solitons exhibit complex behavior, not observed in their nearly 1D counterparts. Notable among the new features are inelastic collisions between solitons, which are strongly sensitive to phase relations between them and their relative speed. An effective 1D Gross-Pitaevskii equation (GPE) including a quintic self-attraction term, which represents deviation from the one dimensionality, makes it possible to explain some of these features [6].

Adding a periodic optical-lattice (OL) potential in the axial direction of the quasi-1D trap makes it possible to create bright matter-wave solitons of the gap type in repulsive condensates [7]. It is a spectacular manifestation of rich dynamics of BEC trapped in OLs, as reviewed in Refs. [8].

Recently, analysis of 2D and 3D localized states in the GPE, that may be stabilized by cellular potentials, i.e., multidimensional OLs, has attracted a great deal of interest, see Ref. [9]. Creation of multidimensional matter-wave solitons is a great challenge to the experiment, as well as the making of spatiotemporal solitons in nonlinear optics [9]. In particular, stable multi-dimensional solitons trapped in a low-dimensional OL (i.e., 1D lattice in the 2D space [10], and 2D lattice in the 3D space [10,11]), have been predicted [10]. As these solitons keep their mobility in the free direction, such settings may be used to test head-on and tangential collisions between solitons. Note that the quasi-1D lattice potential cannot stabilize 3D solitons [10] (this becomes possible if the quasi-1D lattice is combined with the periodic time modulation of the nonlinearity provided by the Feshbach-resonance-management technique [12]; a general account of the technique of periodic management for solitons was given in Ref. [13]).

A low-dimensional OL can also be implemented as a radial (axisymmetric) lattice in both 2D [14–20] and 3D [21] settings. In both cases, stable solitons in the self-attractive medium were predicted, in the form of a spot trapped either at the central potential well, or (in the 2D case) in a radial potential trough (additionally, the so-called azimuthons were predicted as azimuthally periodic deformations of vortices in the uniform 2D medium [22]; however, they are unstable in the case of the cubic nonlinearity). The spot-shaped soliton

may run at a constant angular velocity in the trough, thus being a rotary soliton [14]. The radial-lattice setting may be more convenient for the experimental study of mobility and collisions of matter-wave solitons than the cigar-shaped traps [2,3,5], as in the circular geometry the motion is not affected by the finite size of the longitudinal trap. The radial setting is also appropriate to support patterns in self-repulsive BECs. In particular, dark solitons were created in cigar-shaped traps [1], where the background density is essentially nonuniform, as it vanishes at edges of the trap. In a circular trough, pairs of dark solitons can be created without this complication. In fact, both axisymmetric (azimuthally uniform) vortices [15] and dipole and quadrupole states, that may be regarded as stable complexes of two or four dark solitons [16], were predicted in the two-dimensional GPE with the repulsive nonlinearity and Bessel-lattice radial potential. The stable dipole and quadrupole patterns may also rotate at a constant angular velocity [16].

The aim of this paper is to investigate the existence of localized states in the 2D Gross-Pitaevskii equation with the radially periodic OL potential, $-\varepsilon \cos(2kr)$. In particular, we will show the existence of solitons of the ordinary type in the model with self-attraction, and of radial gap solitons (a new species of solitary waves), in the case of self-repulsion. All localized states reported in this paper have no counterparts in the respective linear equation, being thus different from the above-mentioned solitons in Bessel lattices, which can be obtained by continuation of localized states existing in the linear limit (except for the rotary and 3D solitons). In particular, solitons of the gap type cannot exist in the Bessel-lattice potential, which vanishes at $r \to \infty$.

In addition to the BEC context considered in this paper, similar solitons may also exist in photonic-crystal fibers with a concentric (rather than usual hexagonal) structure, similar to that in fibers with multilayer claddings [23]. In that case, the soliton will be represented by the transverse structure of a self-trapped beam propagating in the fiber.

The paper is organized as follows. In Sec. II we formulate the model based on the two-dimensional GPE. Section III is dealing with solitons trapped in the center (including radial gap solitons, in the case of the repulsive model). In this case, results are obtained in direct simulations, and by means of the variational approximation (VA), both static and dynamical variants of the VA being presented. All subsequent sections deal with annular solitons, which are trapped in ring channels (potential troughs) at a finite distance from the center. Section IV presents approximate analytical results for annular solitons in the attractive model. By means of the VA, we derive an effective 1D equation, which predicts onset of instability of the axisymmetric ring-shaped states against azimuthal modulations. Exact modulated (cnoidal-wave) solutions, which appear above the instability threshold of the axisymmetric state, are found too, as well as exact solutions for azimuthal solitons. Section V addresses the most intriguing issue considered in this work, viz., radial gap solitons (in both cases of attraction and repulsion), with the central lobe trapped in a circular trough. Various types of such solitons are found by means of numerical methods, and it is demonstrated that exactly one of them may be stable, namely, solitons in the repulsive model, which are approximately symmetric about their center in the radial direction. With zero angular momentum ($l=0$), such solitons are completely stable; if $l \neq 0$, the corresponding vortex radial solitons develop small-amplitude rotating azimuthal modulations, and persists indefinitely long in this rotational state. Numerical analysis of radial solitons is further developed in Sec. VI. In particular, the existence of stable annular states with a stationary azimuthal modulation is demonstrated in the attractive model and, in a more general case, it is found that the development of the azimuthal instability of axisymmetric annular solitons in the same model leads to establishment of necklace-shaped patterns consisting of strongly localized (spot-shaped) solitons. Also presented in Sec. VI are stable ring-shaped gap solitons of a large radius in the repulsive model, which carry a pair of dark azimuthal solitons on their crests. Section VII addresses the dynamics of strongly localized solitons moving in circular troughs in the attractive model. It is shown that slowly moving solitons are stable, while fast ones are destroyed due to leakage of matter into the outer trough, under the action of the centrifugal force. Head-on collisions between the moving in-phase solitons in a circular trough lead to collapse (intrinsic blow-up), while π-out-of-phase solitons collide many times, and eventually merge into a single soliton (without loss but collapse); the same happens to in-phase solitons colliding tangentially, if they are trapped in adjacent troughs. Section VIII concludes the paper.

II. THE MODEL

The starting point is the standard GPE in its normalized 2D form [8,13]

$$i\frac{\partial u}{\partial t} = -\left(\frac{\partial^2}{\partial r^2} + \frac{1}{r}\frac{\partial}{\partial r} + \frac{1}{r^2}\frac{\partial^2}{\partial \theta^2}\right)u + V(r)u - \chi|u|^2 u = 0, \tag{1}$$

written for the single-atom wave function u in polar coordinates (r,θ). Here, $\chi=+1$ and -1 correspond to the self-focusing and defocusing nonlinearity, respectively (alias negative and positive scattering length of interatomic collisions) and, as said above,

$$V(r) = -\varepsilon \cos(2kr) \tag{2}$$

is the radially periodic potential; by dint of obvious rescaling, we set $k \equiv 1$. In terms of OLs, this potential can be created by a cylindrical beam whose amplitude is modulated as $\cos(kr)$ (see further discussion below). Note that $\varepsilon > 0$ corresponds to a potential minimum at $r=0$, see an example in Fig. 1 (below, negative values of ε will also be considered, for radial gap solitons in the model with repulsion, $\chi=-1$). Equation (1) can be derived from the following Lagrangian (with an asterisk standing for the complex conjugate):

$$L = \int_0^\infty r dr \int_0^{2\pi} d\theta \left[\frac{i}{2}\left(\frac{\partial u}{\partial t}u^* - \frac{\partial u^*}{\partial t}u\right) - \left(\left|\frac{\partial u}{\partial r}\right|^2 + \frac{1}{r^2}\left|\frac{\partial u}{\partial \theta}\right|^2\right) - V(r)|u|^2 + \frac{1}{2}\chi|u|^4\right]. \tag{3}$$

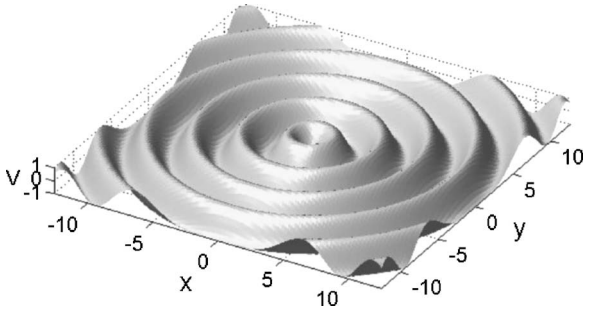

FIG. 1. An example of the radially periodic axisymmetric potential $V(r)=-\cos(2r)$.

Stationary axisymmetric states with chemical potential μ are looked for as solutions to Eq. (1) in the form of $u=U(r)e^{-i\mu t}$, with a real function U obeying the equation

$$\mu U + \left(\frac{d^2}{dr^2} + \frac{1}{r}\frac{d}{dr}\right)U - V(r)U + \chi U^3 = 0. \tag{4}$$

For given potential $V(r)$, solutions to Eq. (4) form families parameterized by μ or, alternatively, by the norm

$$N = 2\pi \int_0^\infty [U(r)]^2 r dr \equiv N = 2\pi \int_0^\infty |u|^2 r dr. \tag{5}$$

Solutions to stationary equation (4) with $\chi=+1$ (self-attraction) were obtained by means of a recently developed spectral-renormalization method for finding self-localized states of nonlinear-Schrödinger (NLS) type equations [24]. Independently, the same stationary solutions were also generated by dint of the well-known method which uses the integration of GPE (1) in imaginary time [25]. Stability of the solitary waves was then tested by adding small perturbations to them and integrating the GPE in real time. A stable perturbed soliton would shed off some radiation, which was absorbed at boundaries of the integration domain, and relax into a slightly different stationary form, corresponding to a smaller norm.

In the case of repulsion ($\chi=-1$), self-localized states were obtained by means of a different numerical technique. In this case, Eq. (1) was solved in real time, with an absorber placed at the boundary of the integration domain. A localized waveform (e.g., Gaussian) with a suitable norm was chosen as the initial condition. In the course of the evolution, excess norm is radiated away with linear waves, which are absorbed at the boundary, and a self-localized state emerges (see the example in Fig. 4 below). It is obvious that solitons found this way are stable.

The abovementioned radial lattices of the Bessel type can be naturally generated by a nondiffracting linear optical beam with the cylindrical symmetry (Bessel beams themselves are usually generated by means of axicoms) [26]. On the other hand, the radial potential of the form of $\cos(2kr)$ can be induced, as said above, by a cylindrical beam whose amplitude is modulated as $\cos(kr)$. The modulation can be provided by passing the cylindrical laser beam through a properly shaped plate [19,20]. Unlike the Bessel beam, one with the $\cos(kr)$ transverse modulation will suffer conical diffraction, but it is not a problem for BEC experiments, as a tight optical trap created in the transverse direction may readily confine a 2D pancake-shaped configuration of the condensate, with thicknesses as small as 2 μm [27]. The diffraction of the paraxial beam, with waist diameter $D\sim 100$ μm, which is a value relevant to the experiment, on such a short propagation distance is completely negligible, as the respective diffraction length (alias Rayleigh range) is estimated to be $z_{\mathrm{diffr}}\sim D^2/\lambda\sim 10$ mm, where $\lambda\sim 1$ μm is the beam's carrier wavelength.

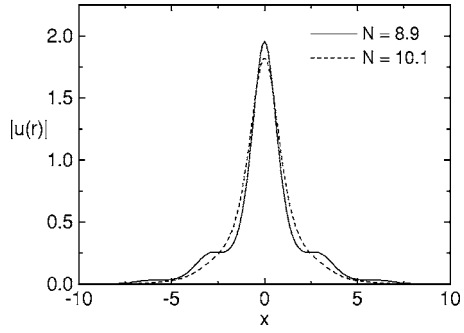

FIG. 2. Axial cross sections of two stable solitons with equal chemical potentials $\mu=-0.5$ trapped (in the model with self-attraction) at the center of the radial structure $V(r)=\varepsilon\cos(2r)$ with $\varepsilon=1.5$ (solid line; in this case, the norm is $N=8.9$) and $\varepsilon=0.5$ (dashed line, corresponding to $N=10.1$).

III. SOLITONS TRAPPED AT THE CENTER

A. Numerical solutions

It is known that a radial potential structure can easily trap a soliton in the central potential well [14]. We start the study of the present model by considering solutions of this type; ring-shaped states, trapped in circular potential troughs at a finite distance from the center, will be considered in subsequent sections. Typical examples of the respective solitonic shape in the model with self-attraction ($\chi=+1$) are displayed in Fig. 2. In the repulsive model ($\chi=-1$), numerical solutions were obtained, as said above, by solving Eq. (1) in real time, in the presence of the boundary absorber. An example of the relaxation of an initial Gaussian pulse into a stable soliton is given in Fig. 3. Full views of the typical stable solitons trapped at the center of the radial structure in the model with self-attraction and self-repulsion are displayed in Fig. 4.

As far as the solitons in the repulsive model ($\chi=-1$) are concerned, a typical example of which is displayed in the lower panel of Fig. 4, they may be clearly classified as solitons of the gap type, since they exist solely due to the interplay of the lattice potential and self-defocusing nonlinearity. The ordinary setting that gives rise to gap solitons is quite similar, with the OL in the 1D, 2D, or 3D Cartesian coordinates [28]. Slowly decaying fringes, attached to the central core of the soliton and evident in the lower panel of Fig. 4 (absent in the ordinary soliton displayed in the upper panel), is a characteristic feature of gap solitons. Thus, this state, self-trapped around the center, may be naturally called a "radial gap soliton."

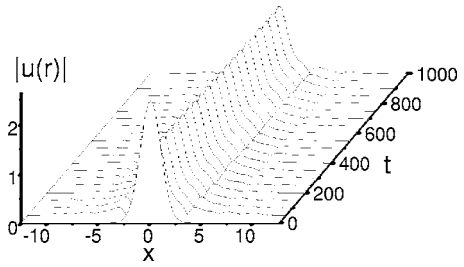

FIG. 3. Formation of a self-trapped state (radial gap soliton) in repulsive BEC around the center of the radial lattice with strength $\varepsilon=3$ (in the presence of absorbers at the boundary of the integration domain) from an initial Gaussian with norm $N=6\pi$. The norm of the eventually established state is $N=5.63$, i.e., $\approx 30\%$ of the initial value.

B. Variational approximation

To describe a stationary soliton trapped in the central potential well in an analytical approximation, we adopt the Gaussian ansatz

$$U(r) = A \exp\left(-\frac{r^2}{2a^2}\right). \tag{6}$$

Comparison with Fig. 2 shows that, in the model with attraction ($\chi=+1$), this ansatz is quite adequate for solitons with a larger norm, trapped in a relatively weak lattice, but it may be inaccurate as an approximation for solitons with smaller N, trapped in a stronger lattice.

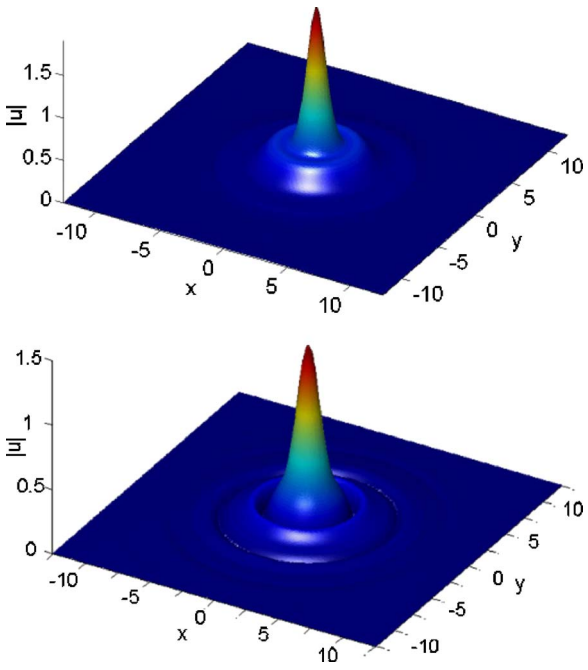

FIG. 4. (Color online) Upper panel: The same localized state in the attractive BEC whose axial cross section is shown by the solid curve in Fig. 2 (with $N=8.9$, $\mu=-0.5$, and $\varepsilon=1.5$). Lower panel: The localized state in the repulsive BEC, with $N=5.63$, $\mu=1.88$, amplitude $A=1.358$, and $\varepsilon=3$, which was generated as shown in Fig. 3.

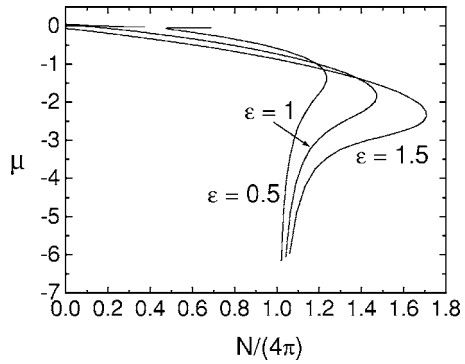

FIG. 5. Dependences $\mu=\mu(N)$ following from variational equations (7), for the self-attraction case $\chi=+1$. According to the VK criterion $d\mu/dN<0$, stable solutions correspond to upper branches of the curves.

The application of the variational approximation (VA) to stationary equation (4), with the accordingly modified Lagrangian (3), is straightforward (see Refs. [10,29,30], where the same Gaussian ansatz was used to predict 2D solitons trapped in quasi-1D and square 2D OLs). Thus we arrive at VA-generated equations, that relate the soliton's size a to its norm and chemical potential

$$\frac{\chi N}{4\pi} = 1 - \frac{1}{2}\varepsilon a^3 \frac{df}{da}, \quad \mu = \varepsilon\left[a\frac{df}{da} + f(a)\right] - \frac{1}{a^2}, \tag{7}$$

where $f(a)=1-\sqrt{\pi}ae^{-a^2}\mathrm{erfi}(a)$, $\mathrm{erfi}(a)\equiv \mathrm{erf}(ia)/i$ is a real function, and erf is the standard error function.

The analysis of dependence $\mu=\mu(N)$ following from Eqs. (7) with $\chi=+1$ (self-focusing) predicts the existence of a family of solitons trapped at the center of the radial lattice, which are stable according to the Vakhitov-Kolokolov (VK) stability criterion [31,32], $d\mu/dN<0$, as shown in Fig. 5. Although the VK criterion is only necessary for the stability, as it ignores a possibility of oscillatory instability with complex eigenvalues, direct simulations of Eq. (1) confirm the stability of these solutions (see below).

Additional evidence for the existence of self-trapped localized states of BEC in the present model can be provided by a more general, time-dependent, version of the VA. To this end, we define a generalized ansatz [see Eq. (6)]

$$u(r,t) = A(t)\exp\left[-\frac{r^2}{2[a(t)]^2} + \frac{i}{2}b(t)r^2 + i\phi(t)\right], \tag{8}$$

where b is a real radial chirp, and ϕ is the overall phase. Applying the standard VA procedure [33], one arrives at the following evolution equation for the width of the localized state:

$$\frac{d^2a}{dt^2} = \frac{4(1-\chi')}{a^3} + 2\varepsilon[2a + \sqrt{\pi}(1-2a^2)e^{-a^2}\mathrm{erfi}(a)], \tag{9}$$

where an effective nonlinearity strength is

$$\chi' \equiv \chi N/(4\pi), \tag{10}$$

and the amplitude of ansatz (8) is given by

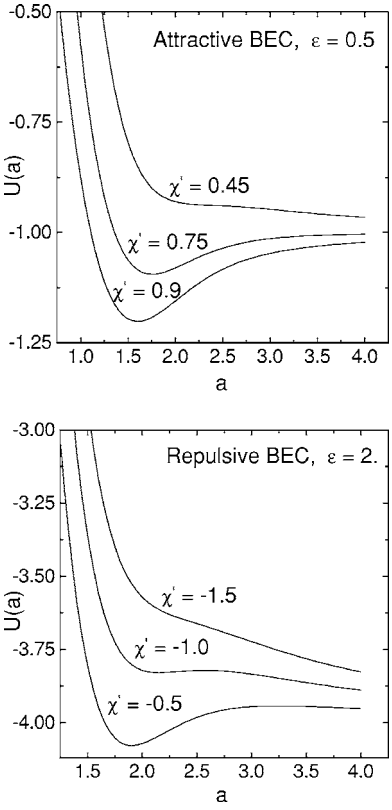

FIG. 6. The variational potential, as given by Eq. (12) for different values of $\chi' = \chi N/(4\pi)$, at fixed strength ε of the radial optical lattice.

$$A^2(t) = N/[\pi a^2(t)]. \tag{11}$$

Equation (9) describes motion of a unit-mass particle with coordinate $a(t)$ in the effective potential

$$U(a) = \frac{2(1-\chi')}{a^2} - 2\sqrt{\pi}\varepsilon a e^{-a^2}\mathrm{erfi}(a). \tag{12}$$

In Fig. 6 the effective potential (12) is depicted for different values of χ', for the attractive and repulsive versions of the model.

Solitons in the attractive BEC ($\chi=+1$) exist when potential (12) possesses a local minimum. In particular, for $\varepsilon=0.5$ (see Fig. 6), the potential minimum exists provided that $\chi' > 0.45$. For the norm smaller than that corresponding to $\chi'=0.45$ [see Eq. (10)], the self-attraction is too weak to form a soliton, and the matter-wave pulse spreads out through barriers of the radial potential. On the other hand, in the case of attraction, χ' is also limited from above, by the collapse occurring at a critical value, $\chi'_{\mathrm{cr}}=N_{\mathrm{cr}}/(4\pi)$. In the absence of the lattice ($\varepsilon=0$), a numerically found critical norm is $N_{\mathrm{cr}}^{(0)} \approx 11.7$ (it is equal to the norm of the Townes soliton) [32]. For any ε, the VA predicts $\chi'_{\mathrm{cr}}=1$, as the value of coefficient χ' at which the first term in effective potential (12) vanishes. According to Eq. (10), this gives $N_{\mathrm{cr}}^{(\mathrm{var})}=4\pi$ [34], to be compared to the above-mentioned numerical value 11.7.

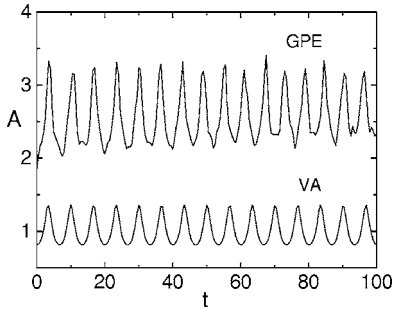

FIG. 7. Comparison of a result of the variational approximation (VA) with direct simulations of Eq. (1) (GPE) with $\chi=+1$ (the attractive model), in terms of the soliton's amplitude as a function of time. Intrinsic vibrations of the soliton were triggered by sudden increase of the lattice strength from $\varepsilon=0.5$ to $\varepsilon=0.75$, for the state self-trapped around the center, with $N=10.1$ in Fig. 2.

Thus, the VA predicts a finite existence region for stable localized states self-trapped at the center of the radial lattice in the attractive BEC; for example, it is $0.45<\chi'<1$ for $\varepsilon=0.5$. While the upper edge of this region is fixed, as said above, at $N=N_{\mathrm{cr}}^{(\mathrm{var})}=4\pi$, numerical analysis of expression (12) demonstrates that the lower critical norm necessary for the existence of the self-trapped state, as predicted by the VA, almost linearly decreases with the increase of the OL strength ε. Numerical solution of the axisymmetric version of GPE (1) demonstrates that, although the collapse sets in at

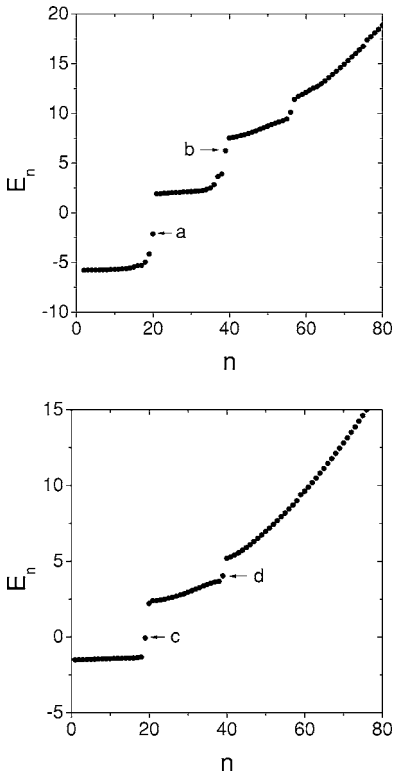

FIG. 8. Upper panel: Energy levels (eigenvalues of chemical potential μ) found from full nonlinear equation (33) with $\chi=+1$ (attraction) for $l=10$ and $\varepsilon=-10$ ($\varepsilon<0$ means the presence of a potential maximum at $r=0$). Lower panel: The same, but for the repulsive model $\chi=-1$, with $l=2$ and $\varepsilon=4$.

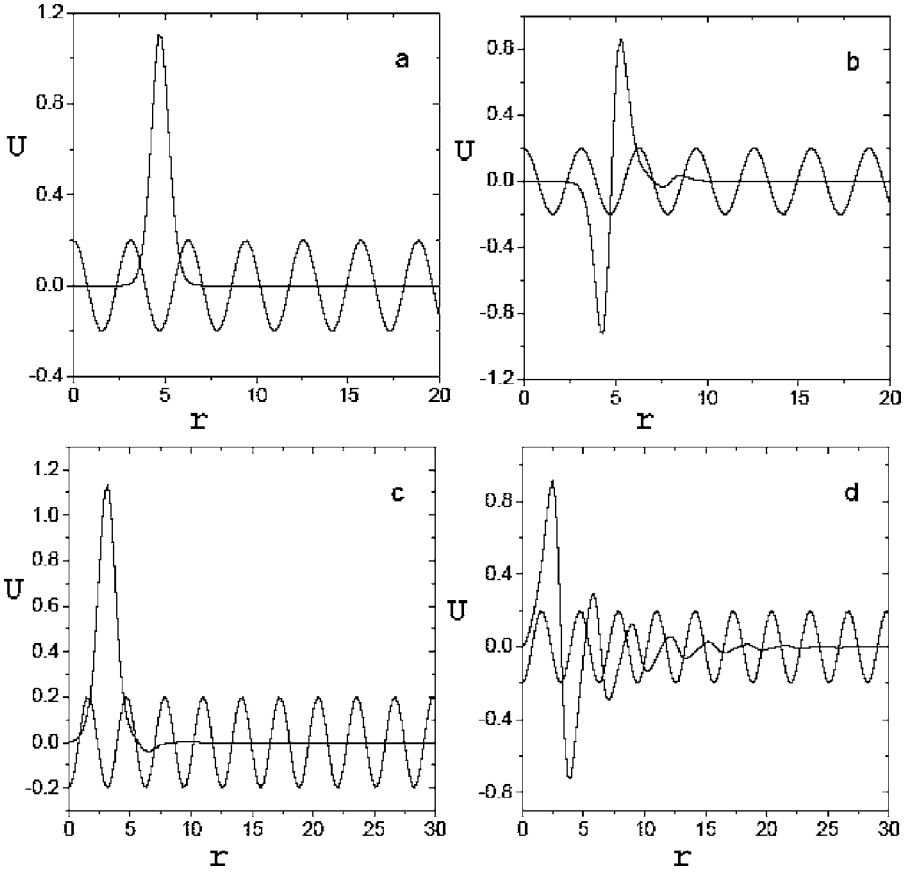

FIG. 9. (a), (b) Radial (annular) gap solitons (thick lines), trapped in the circular trough of the potential around $r=1.5\pi$, in the attractive model ($\chi=+1$). The solitons correspond, respectively, to eigenvalues of chemical potential μ marked by "a" and "b" in the left panel of Fig. 8, which are $\mu_a=-2.1277$ and $\mu_b=6.0543$. Panels (c) and (d) display radial gap solitons in the repulsive model ($\chi=-1$), trapped in the circular trough of the potential around $r=\pi$. These solitons appertain, respectively, to eigenvalues "c" and "d" marked in the right panel of Fig. 8, $\mu_c=-0.07359$ and $\mu_d=4.09066$. All solitons shown in this figure have norm $N=10\pi$. Thin lines depict the radial potential proper $-\varepsilon\cos(2r)$ scaled by a factor of 50 in (a), (b), and by 20 in (c), (d).

a critical value of the norm which, in the presence of the radial OL, is slightly higher than $N_{\rm cr}^{\rm (var)}=4\pi$, similar to the case of the 2D soliton stabilized by the quasi-1D or square OL [10,29,30], the dependence of $N_{\rm cr}$ on ε is weak. The physical mechanism behind the rise of the collapse threshold in a trapping potential is that the confinement allows the soliton to increase the internal "quantum pressure," generated by the dispersion term in GPE (1), which counteracts the nonlinear self-focusing of the wave packet.

Predictions of the VA for dynamical regimes can be compared to direct simulations in terms of the time dependence of the amplitude, $A(t)$, in a solution which was excited by a sudden perturbation [the variational prediction for $A(t)$ is taken as per Eq. (11)]. To display an example, we take the stationary solution from Fig. 2, corresponding to $\varepsilon=0.5$ and $N=10.1$, and suddenly increase the lattice strength to $\varepsilon=0.75$. Comparison of the variational results with simulations of Eq. (1) is presented in Fig. 7. It is observed that the agreement for absolute values of the amplitude is only qualitative, while the oscillation frequencies coincide better.

In the case of the repulsive BEC ($\chi=-1$), the behavior is opposite, as seen in the right panel of Fig. 6. In this case, a larger norm for given OL strength ε causes spreading of the localized state, because the self-defocusing nonlinearity overcomes the confining effect of the trapping potential. Simulations of Eq. (1) with $\chi=-1$ show that the wave packet sheds off excessive norm in the form of linear waves, which are absorbed at domain boundaries, and relaxes into a stable shape after the norm becomes appropriate. For example, at $\varepsilon=2$ stable localized states in the repulsive BEC exist at $|\chi'|\lesssim 1$ [i.e., the norm is limited to values $N\lesssim 4\pi$, see Eq. (10)].

IV. RING-SHAPED SOLITONS: AN ANALYTICAL APPROACH

A. Variational approximation

An essential property of radially periodic potentials is that localized states can self-trap not only in the central potential well, but also in remote circular troughs [14,16]. These localized states are the subject of the consideration in the rest of the paper. If the trough's curvature is small, then states resemble 2D solitons in the quasi-1D OL reported in Ref. [10]. First, we aim to derive an asymptotic 1D equation for patterns trapped in a circular trough, and obtain its relevant solutions. To this end, we adopt the following ansatz for the solution:

$$\psi(r,\theta,t)=\sqrt{2}A(y,t)\,\mathrm{sech}(x/\rho), \tag{13}$$

where $y\equiv r_0\theta$ is the coordinate running along the circumference of radius r_0, $A(y,t)$ is a slowly varying complex amplitude, and the transverse variable is $x\equiv r-\pi m$, with $r_0\equiv\pi m$ being a radial potential minimum in a vicinity of which the ring-shaped pattern is trapped. Assuming that m is large enough, we consider the annular pattern placed in a remote circular trough, which may be treated as a quasi-rectilinear potential trap, with negligible curvature. Obviously, the latter condition amounts to $\rho\ll r_0$ [recall ρ is the radial size in ansatz (13)].

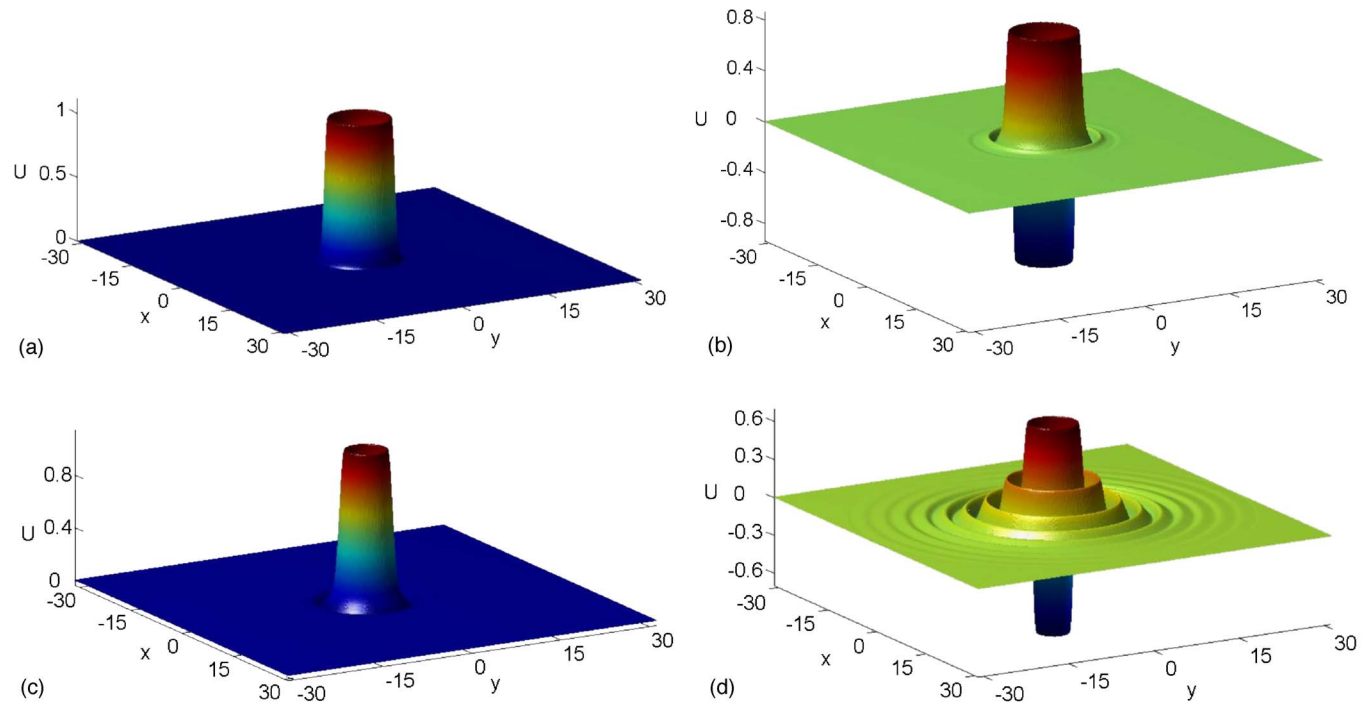

FIG. 10. (Color online) Left and right top panels: 3D view of the annular gap solitons corresponding to bound states (a) and (b), respectively, of Fig. 9. Left and right bottom panels: The same for bound states (c) and (d) from Fig. 9.

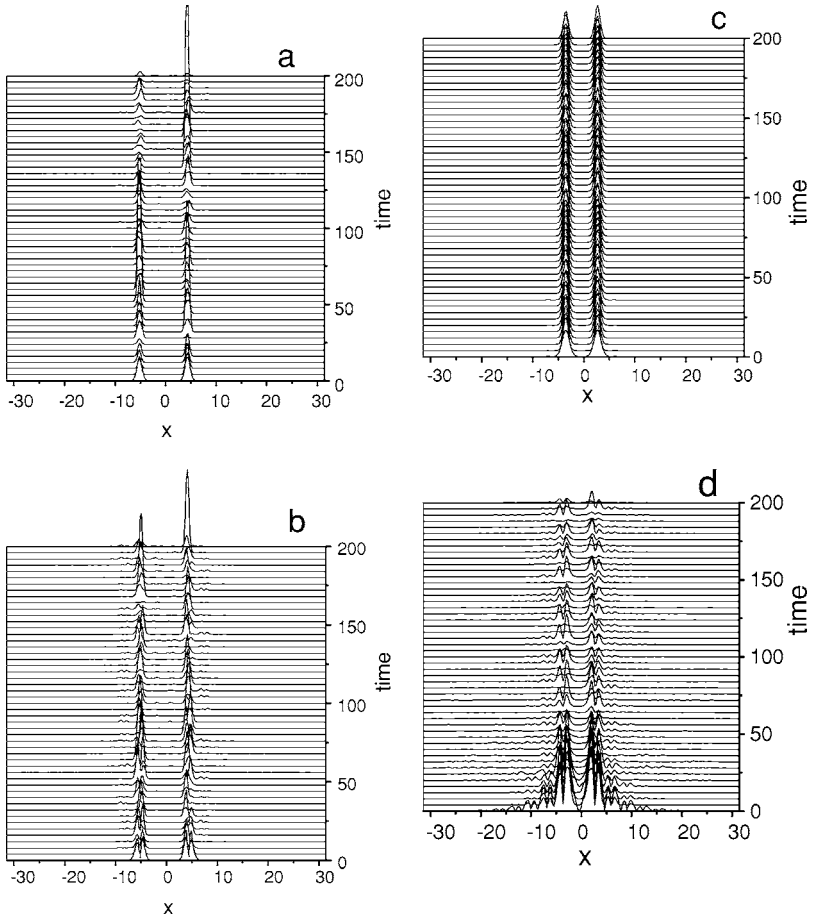

FIG. 11. Time evolution of the density $|u(x,y,t)|^2$ in cross section $y=0$, obtained from simulations of Eq. (31) with initial conditions taken as slightly perturbed localized states from panels (a)–(d) of Fig. 9. Parameters are the same as in the respective panels of Fig. 8. Panels (a), (b), and (d), which pertain, respectively, to the attractive and repulsive models, represent unstable types of annular gap solitons. On the contrary, in panel (c) the gap soliton of the onsite symmetric type (in terms of its radial structure), with angular momentum $l=2$, remains, as a matter of fact, stable in the repulsive model, just developing a small azimuthal modulation which travels along its crest, making the entire pattern rotating. The rotation manifests itself through unequal and varying in time heights of the two humps and spacings between them.

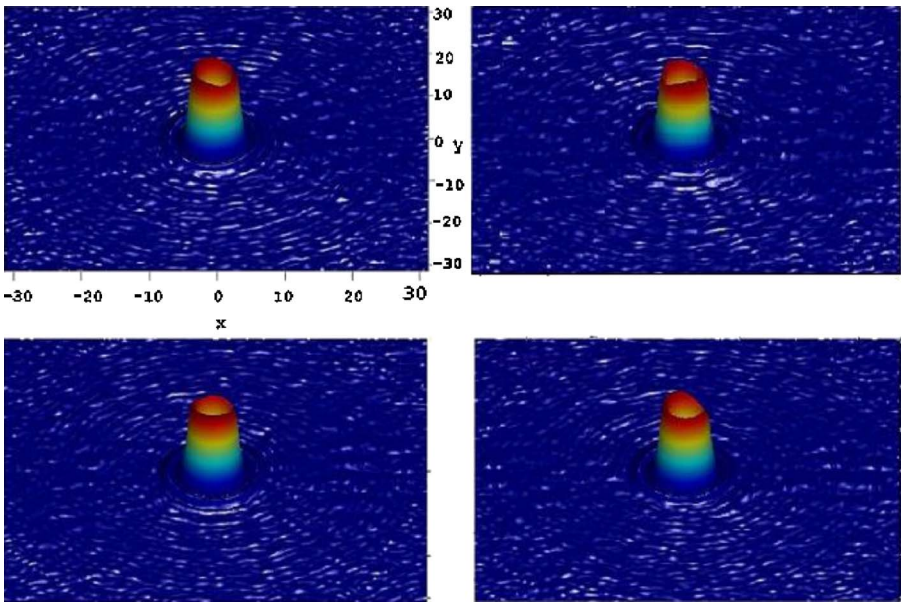

FIG. 12. (Color online) Snapshots of the perturbed annular gap solitons from Fig. 11(c) taken at times $t=28.75$, 30.50, 32.25, 34.00 and set in the clockwise direction, starting from the top left panel. Scales along the axes are the same as in the top left panel.

Neglecting the curvature in Eq. (1), we rewrite it as a 2D equation with x and y treated as local Cartesian coordinates

$$i\frac{\partial\psi}{\partial t}+\frac{\partial^2\psi}{\partial x^2}+\frac{\partial^2\psi}{\partial y^2}+\chi|\psi|^2\psi+\varepsilon\cos(2x)\psi=0. \quad (14)$$

The next step is to reduce Eq. (14) to an effectively 1D equation along azimuthal direction y. To this end, we note that Eq. (14) can be derived from the Lagrangian [see Eq. (3)]

$$L=\int\int dxdy\left[\frac{i}{2}(\psi_t\psi^*-\psi\psi_t^*)-(|\psi_x|^2+|\psi_y|^2)+\frac{1}{2}\chi|\psi|^4+\varepsilon\cos(2x)|\psi|^2\right].$$

We substitute ansatz (13) in this Lagrangian, and integrate the resulting expression in transverse direction x, which yields an effective (averaged) Lagrangian

$$L_{\text{eff}}=2\int_{-\infty}^{+\infty}dy\left[i\rho(A_tA^*-AA_t^*)-2\rho|A_y|^2-2I\frac{\rho_y^2}{\rho}|A|^2-\frac{2|A|^2}{3\rho}+\frac{4}{3}\chi\rho|A|^4+\frac{2\pi\varepsilon\rho^2|A|^2}{\sinh(\pi\rho)}\right], \quad (15)$$

where $I\equiv\int_0^{+\infty}(\text{sech}^2x-\text{sech}^4x)x^2dx\approx0.61$.

The application of the standard variational procedure to averaged Lagrangian (15) gives rise to a cumbersome system of coupled equations for the complex amplitude $A(y,t)$ and real width $\rho(y,t)$. The equations strongly simply if we assume that A and ρ are slowly varying functions of y, that, in particular, corresponds to long-wave perturbations which account for the onset of the modulational instability (MI), see below. Further, in the attractive model ($\chi=+1$), one may first look for a stationary solution, completely neglecting the y dependence and assuming time independent $|A|$ and ρ. These assumptions give rise to a result previously known from the application of the VA to the 1D NLS equation with potential $\cos(2kx)$ [35],

$$|A|=\sqrt{\frac{1}{\rho^2}-\frac{3}{2}\varepsilon\pi\rho\left[\pi\rho\frac{\cosh(\pi\rho)}{\sinh^2(\pi\rho)}-\frac{1}{\sinh(\pi\rho)}\right]}. \quad (16)$$

This relation is cumbersome too, but straightforward analysis demonstrates that it takes a very simple form $|A|=1/\rho$ when ε is either small or large [in the latter case, scaling $|A|\sim\rho^{-1}\sim\sqrt{\varepsilon}$ holds, lending the last three term in the Lagrangian density in Eq. (15) the same order of magnitude].

To obtain a closed-form Lagrangian for the nonstationary (but slowly varying) amplitude field $A(y,t)$ in the attractive model, one should express ρ in Eq. (15) in terms of $|A|$, using relation (16). This will lead, in the general case, to a messy result; however, the abovementioned simplest ap-

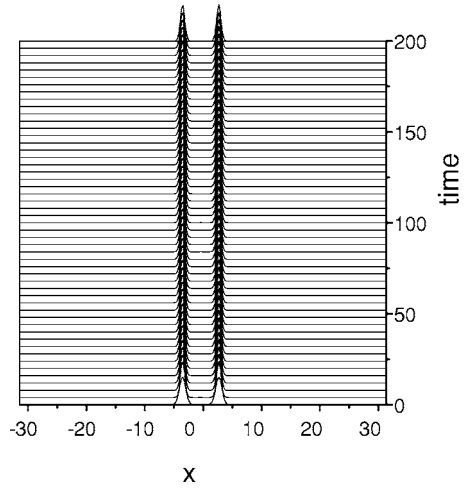

FIG. 13. Time evolution (in the $y=0$ cross section) of $|u(x,y,t)|^2$ of a perturbed annular gap soliton with $l=0$ of the onsite symmetric type, in the repulsive model $\chi=-1$, with $\varepsilon=10$. All solitons of this type (with $l=0$) are found to be stable.

proximation $\rho=1/|A|$, which replaces Eq. (16), yields a tractable expression

$$L_{\rm eff}=2\int_{-\infty}^{+\infty}dy\left\{i\left(A_t\sqrt{\frac{A^*}{A}}-A_t^*\sqrt{\frac{A}{A^*}}\right)+\frac{4}{3}|A|^3 - \frac{I}{2}\left[\frac{(A_y^*)^2}{A^*}\sqrt{\frac{A}{A^*}}+\frac{A_y^2}{A}\sqrt{\frac{A^*}{A}}\right]-(2+I)\frac{|A_y|^2}{|A|}+2\varepsilon|A|\right\} \tag{17}$$

[the last term in the Lagrangian density should be dropped if ε is small; if, on the contrary, ε is large, the term is obtained within the framework of the above scaling, that assumes small ρ, hence $\sinh(\pi\rho)\approx\pi\rho$ in Eq. (15)]. Finally, Lagrangian (17) gives rise to the following Euler-Lagrange equation, $\delta S/\delta A^*=0$:

$$i\tilde{A}_t+(2+I)\tilde{A}_{yy}-\left(1+\frac{3I}{4}\right)\frac{\tilde{A}_y^2}{\tilde{A}}+I\left[\frac{\tilde{A}}{\tilde{A}^*}\tilde{A}_{yy}^* + \frac{|\tilde{A}_y|^2}{2\tilde{A}^*}-\frac{3}{4}\frac{(\tilde{A}_y^*)^2\tilde{A}}{(\tilde{A}^*)^2}\right]+2|\tilde{A}|^2\tilde{A}=0, \tag{18}$$

where the transformation $\tilde{A}(y,t)\equiv A(y,t)e^{i\varepsilon t}$ was used to eliminate a linear term in the equation generated by the last term in Lagrangian (17). Equation (18) with $I=0$ also appears in connection with a model describing the propagation of surface waves on a plasma layer with a sharp boundary [36].

Stationary solutions to Eq. (18) with chemical potential μ are looked for in the ordinary form $\tilde{A}(y,t)=e^{-i\mu t}B(y)$, with $B(y)$ satisfying equation

$$(1+I)\left[2\frac{d^2B}{dy^2}-\frac{1}{B}\left(\frac{dB}{dy}\right)^2\right]+2B^3+\mu B=0, \tag{19}$$

which can be derived from the respective Hamiltonian $H=(2/3)B^3+\mu B+(1+I)(dB/dy)^2/B$. Setting $H=0$, one obtains a family of soliton solutions to Eq. (19), for any $\mu<0$:

$$B_{\rm sol}(y)=\sqrt{-\frac{3\mu}{2}}\,\mathrm{sech}\left(\sqrt{-\frac{\mu}{1+I}}y\right). \tag{20}$$

For $H<0$ and $\mu<0$, a family of periodic cnoidal-wave solutions to Eq. (19) is obtained in the form of

$$B_{\rm cn}(y)=\frac{B_0B_1}{B_1+(B_0-B_1)\mathrm{cn}^2\left(\sqrt{\frac{B_0(B_1+|B_2|)}{6(1+I)}}y,q\right)}, \tag{21}$$

where $\mathrm{cn}(z,q)$ is the Jacobi's elliptic cosine, with modulus

$$q=\sqrt{\frac{B_0-B_1}{B_0}\frac{|B_2|}{B_1+|B_2|}}<1, \tag{22}$$

and $B_2<0<B_1<B_0$ are three roots of equation $(2/3)B^3+\mu B-H=0$. Solutions (21) exist, for given $\mu<0$, in a region of $0\le -H\le(\sqrt{2}/3)|\mu|^{3/2}$; as said above, the limit of $H=0$ corresponds to soliton (20), while the opposite limit $H=-(\sqrt{2}/3)|\mu|^{3/2}$, corresponds to a uniform CW (continuous-wave) solution, with

$$B_0=B_1\equiv B(y)=\sqrt{|\mu|/2},\quad B_2=-\sqrt{2|\mu|}. \tag{23}$$

Cnoidal solutions on the ring of radius r_0 must satisfy the corresponding periodic boundary conditions (BCs), $\tilde{A}(y,t)=\tilde{A}(y+2\pi r_0,t)$ (for the ordinary 1D NLS equations with repulsion and attraction, analytical solutions satisfying the periodic bcs were studied in Refs. [37,38], respectively). Accordingly, parameter H in solutions (21), (22) is not a continuously varying one, but rather takes discrete values selected by matching the BC to the periodicity of cn^2,

$$\frac{\pi r_0}{n}=\sqrt{\frac{6(1+I)}{B_0(B_1+|B_2|)}}K(q), \tag{24}$$

where K is the complete elliptic integral, and n is an arbitrary integer.

Note that Eq. (18) features the Galilean invariance: if $\tilde{A}(y,t)$ is a solution, then its counterpart in the form of a solution moving at an arbitrary velocity v is

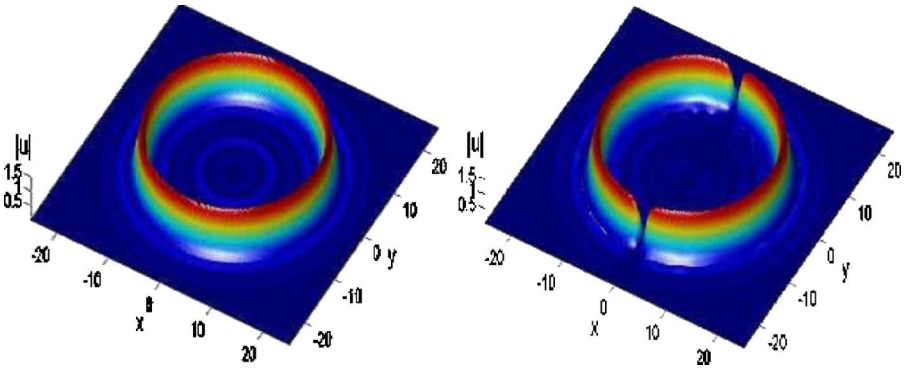

FIG. 14. (Color online) Left panel: An example of a stable annular gap soliton (with $l=0$) in the repulsive model with $\varepsilon=3$. The center of the soliton is located in a remote trough, around $r_0=5\pi$. The norm and chemical potential of this soliton are $N=344.3$ and $\mu=0.78$. Right panel: A stable configuration formed by two azimuthal dark solitons created on top of an annular gap soliton shown in the left panel. This state has norm $N=330.6$ and chemical potential $\mu=0.80$.

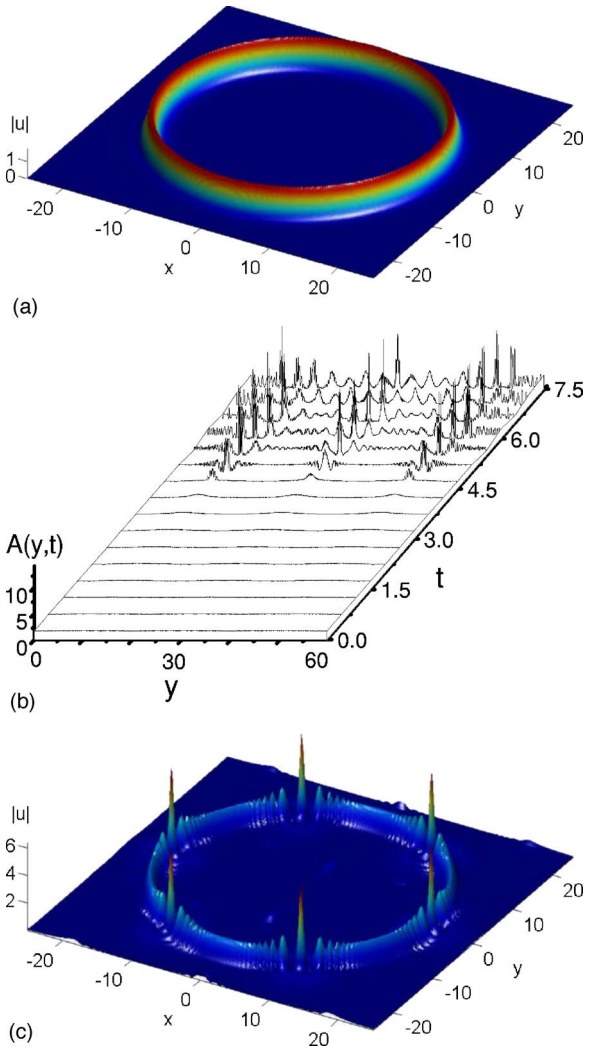

FIG. 15. (Color online) (a) An unstable ring-shaped soliton in the attractive model with $\varepsilon=2$, trapped in a circular trough around $r_0=6\pi$ (the soliton was found by means of the imaginary-time integration). The amplitude of this soliton is 1.8, and its chemical potential and norm are $\mu=-2.3$ and $N=420$ [the analytical approximation (28) predicts $N=426$ in this case]. The modulational instability (MI) of this axisymmetric state is correctly predicted by Eq. (29). (b) Development of the MI, triggered by a small azimuthal perturbation, $\delta u=0.02\cos(6\phi)\exp[-(r-r_0)^2/2]$. The evolution is shown in terms of the amplitude, $|u(y,t)|$, taken along circumference $y=r_0\theta$, with $r_0=6\pi$ and θ running from 0 to π (due to the symmetry, only half of the circle is shown). (c) The field profile formed at time $t=5$, demonstrating the emergence of a regular necklace-shaped pattern.

$$\tilde{A}_c(y,t)=\tilde{A}(y-vt)\exp\left(\frac{i}{4}vy-\frac{i}{2}v^2t\right), \tag{25}$$

hence one can boost solitons (20) and cnoidal waves (21) to a (formally) arbitrary velocity by means of transformation (25). In fact, the velocity is not arbitrary because the factor $\exp(ivy/4)$ also must satisfy the periodic BC, which leads to the velocity-quantization condition $v=4n/r_0$, with $n=0,\pm1,\pm2,\ldots$.

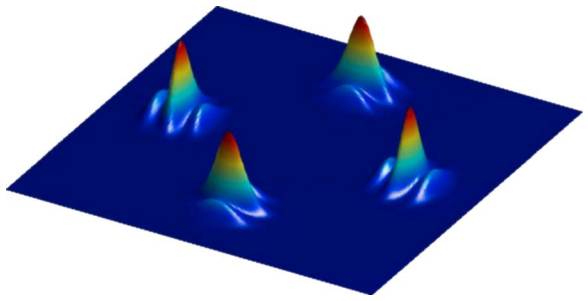

FIG. 16. (Color online) A stable necklace pattern composed of four strongly localized solitons in the attractive model with $\varepsilon=2$, trapped
in a circular trough around $r_0=5\pi$. The norm of each soliton is $N=2\pi$, with the phase difference of π between adjacent ones. The radial lattice is embedded in an integration domain of size $16\pi\times16\pi$.

B. Modulational instability of the uniform ring soliton in the model with attraction

In the model with attraction ($\chi=+1$), the existence of uniform ring-shaped solitons trapped in annular troughs of large radii is obvious, while a nontrivial issue is a possibility of finding a stability region for such solutions. In terms of Eq. (18), the ring soliton is represented by a continuous-wave (CW) solution with a constant amplitude B_0, which was mentioned above as a limit case of the cnoidal solution family, with $\mu=-2B_0^2$.

It is well known that, while all CW solutions of NLS-like equations with attraction are modulationally unstable in the infinite domain, periodic bcs may stabilize them if the CW amplitude is smaller than a certain critical value. This argument suggests a possibility to find a stability region for the uniform ring solitons in the present model with attraction.

A standard analysis of the MI assumes a perturbation of the CW solution

$$\tilde{A}(y,t)=[B_0+B_1(y,t)]\exp[2iB_0^2t+i\chi_1(y,t)],$$

with infinitesimal amplitude and phase perturbations B_1 and χ_1. Eigenmodes of the perturbations may be looked in the form proportional to $\exp(ipy+\gamma t)$, where p is an arbitrary

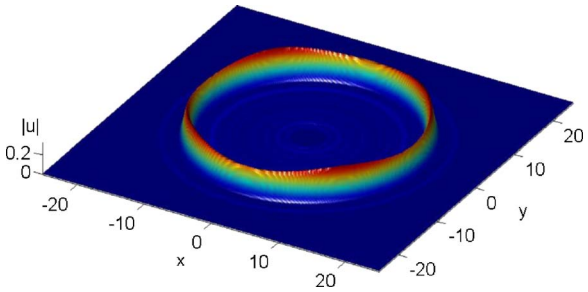

FIG. 17. (Color online) A stable ring-shaped soliton featuring weak azimuthal modulation, in the model with attraction and strong radial lattice ($\varepsilon=10$). The solution's norm and chemical potential are $N=7.2$ and $\mu=-5.7$.

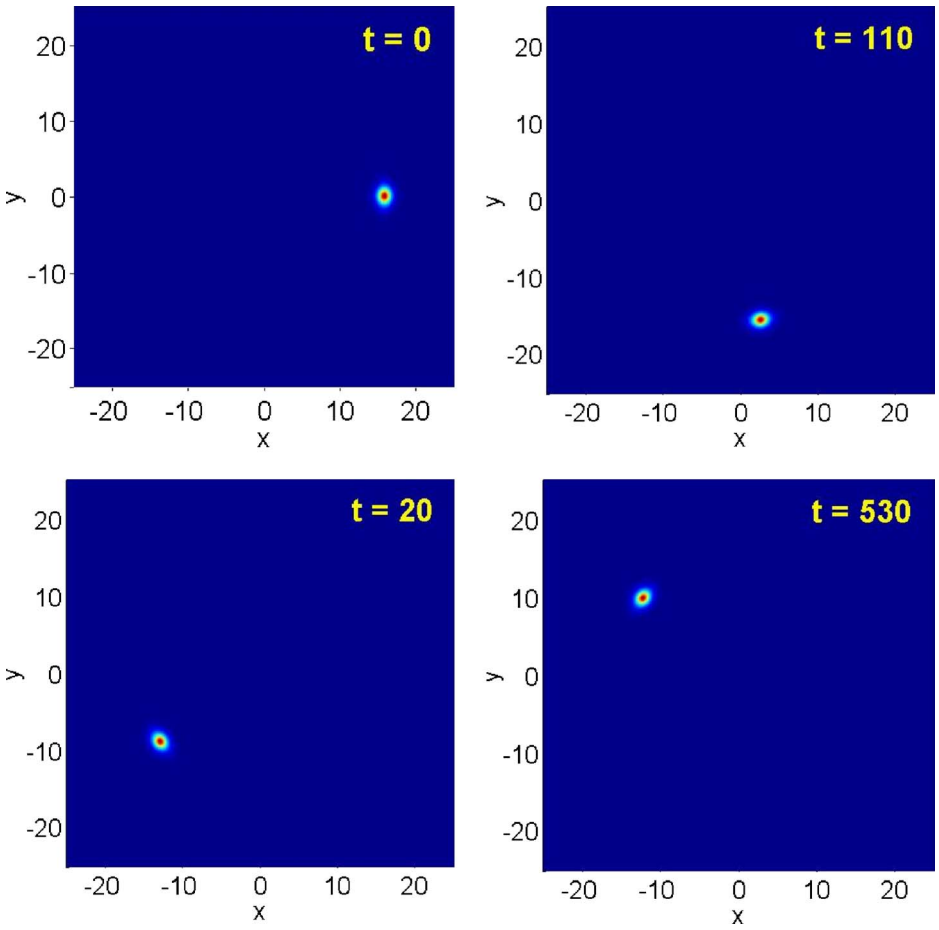

FIG. 18. (Color online) A stable strongly localized soliton in the attractive model, with norm $N=9.42$, trapped in the circular trough around $r_0=5\pi$, was set in motion in the clockwise direction with velocity $v=1$. As illustrated by the sequence of snapshots, the circular motion in the trough continues indefinitely long without any visible loss.

real wavenumber, and γ is the corresponding instability growth rate. Straightforward calculations demonstrate that the CW solution to Eq. (18) is subject to the MI under condition

$$p^2[2B_0^2-(1+I)p^2]>0. \tag{26}$$

In the annular system that we are dealing with, p is subjected to the geometric quantization, the same way as above, i.e., $p=n/r_0$ with integer n. Therefore, condition (26) with lowest $|n|=1$ is not satisfied, giving one a chance to make the CW solution modulationally stable, under the condition

$$2B_0^2r_0^2\leq 1+I. \tag{27}$$

In a final form, this stability condition may be expressed in terms of the full norm of the axisymmetric ring soliton. Substituting ansatz (13) in Eq. (5), and making use of the assumptions adopted above, one obtains $N\approx 8\pi r_0\rho B_0^2$. Further, substituting here the above approximation, $\rho=1/B_0$, yields

$$N=8\pi r_0B_0. \tag{28}$$

With regard to this relation, stability condition (27) amounts to a limitation on N:

$$N<N_{\rm thr}=4\sqrt{2(1+I)}\pi\approx 22.55. \tag{29}$$

A natural way to look at these stability conditions is to consider a situation with gradually increasing N (or B_0). The azimuthally uniform ring solution will loose its stability when the amplitude (or norm) attains the critical value defined by Eq. (27) [or by Eq. (29)]. One may expect that the onset of the MI gives rise to a bifurcation, which creates stable azimuthally modulated solutions, with a modulation depth scaling as $\sqrt{N-N_{\rm thr}}$ for $0<(N-N_{\rm thr})/N_{\rm thr}\ll 1$. Alternatively, one may fix the CW amplitude B_0 and gradually increase the trough's radius r_0; the loss of the CW stability and emergence of the modulated solutions should occur when r_0 attains a critical value following from Eq. (27),

$$(r_0)_{\rm cr}=\sqrt{(1+I)/2}B_0^{-1}. \tag{30}$$

In fact, the modulated states generated by the onset of the MI should be nothing else but the stationary cnoidal wave given by Eqs. (21) and (22). Indeed, with regard to Eq. (23) and the fact that $K(0)=\pi/2$, it follows from matching condition (24) that, with the increase of r_0 for fixed B_0, the cnoidal-wave solution appears, with an infinitely small modulation depth, at $r_0=(r_0)_{\rm cr}$, where the critical value $(r_0)_{\rm cr}$ is precisely the same as defined by the onset of the MI [i.e., given by Eq. (30)].

A defect of the above approximate analysis is that, with regard to relation $A_0=1/\rho$, stability condition (29) may be cast in the form of $\rho/r_0>\sqrt{2/(1+I)}\approx 1.1$, which does not comply with the underlying low-curvature assumption $\rho_0\ll r_0$. This fact makes the existence of modulationally stable ring-shaped solitons in the present model with attrac-

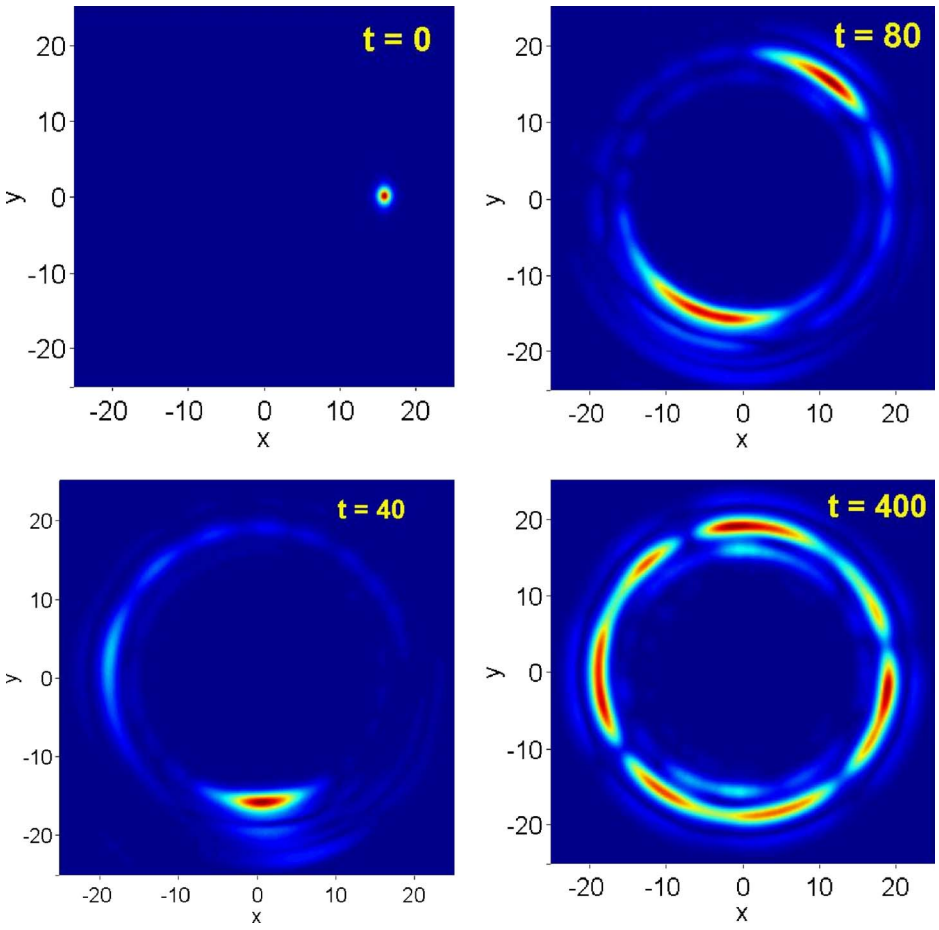

FIG. 19. (Color online) If the same soliton as in Fig. 18 (with initial norm $N=9.42$) is set in motion with a greater velocity $v=3$, the centrifugal force gives rise to the underbarrier leakage of atoms into outer circular troughs. As illustrated by the sequence of snapshots, the decaying soliton cannot preserve its shape. The norm remaining within the given radial channel at $t=400$ is $N_{\text{final}} \simeq 0.5$, i.e., $\simeq 5\%$ of the initial value.

tion doubtful (note that the linear approximation does not suggest the existence of such stable states either, as the radially periodic potential does not support localized states in the respective linear Schrödinger equation). In direct simulations of Eq. (1) with $\chi=+1$, we were unable to find modulationally stable azimuthally uniform nonlinear states. However, stable azimuthally modulated states, similar to those predicted above in the form of Eq. (21), have been found indeed, as reported below in Sec. VI B.

V. ANNULAR GAP SOLITONS

In this section we address the central issue concerning the nonlinear dynamics of matter waves in the radially periodic potential given by Eq. (2), viz., the bandgap spectrum of the model and a possibility of the existence of annular gap solitons (in both the attractive and repulsive models, $\chi=\mp 1$), with their centers located in circular troughs, far enough from the center. Thus, we consider the following 2D GPE [recall we adopt the normalization corresponding to $k=1$ in Eq. (2)]:

$$iu_t = -\left(\frac{\partial^2}{\partial r^2} + \frac{1}{r}\frac{\partial}{\partial r} + \frac{1}{r^2}\frac{\partial^2}{\partial \theta^2}\right)u - \varepsilon \cos(2r)u - \chi|u|^2 u. \tag{31}$$

We look for ring-shaped solutions to Eq. (31) as

$$u(r,\theta,t) = \phi(r)e^{-i\mu t + il\theta}, \tag{32}$$

where $l=0,1,2,\ldots$, is the vorticity of the radial soliton. Real function $\phi(r)$ is to be found from equation

$$\frac{d^2\phi}{dr^2} + \frac{1}{r}\frac{d\phi}{dr} + [\mu + \varepsilon \cos(2r)]\phi + \left(\chi\phi^2 - \frac{l^2}{r^2}\right)\phi = 0.$$

By dint of the known transformation $\phi(r) \equiv r^{-1/2}U(r)$, this equation is reduced to an effective 1D eigenvalue problem, based on the following equation:

$$\frac{d^2U}{dr^2} + \left[\mu + \varepsilon \cos(2r) + \left(\chi\frac{U^2}{r} - \frac{l^2+1/4}{r^2}\right)\right]U = 0. \tag{33}$$

In the limit of $r \to \infty$, the linearized version of Eq. (33) coincides with the linear Mathieu equation, with its well-known bandgap structure. However, the part of the spectrum associated with excitations localized at finite r may be strongly affected by the centrifugal barrier present in Eq. (33).

To investigate the band structure and gap solitons of Eq. (33), we used a self-consistent method developed in Ref. [39]. Stability of gap solitons obtained by means of this method was then tested, using the solitons as initial conditions for simulations of Eq. (31) in real time. In Fig. 8, we depict lower parts of the spectrum of energy eigenvalues for axisymmetric states, as found from the effective nonlinear stationary equation, Eq. (33), with the attractive and repul-

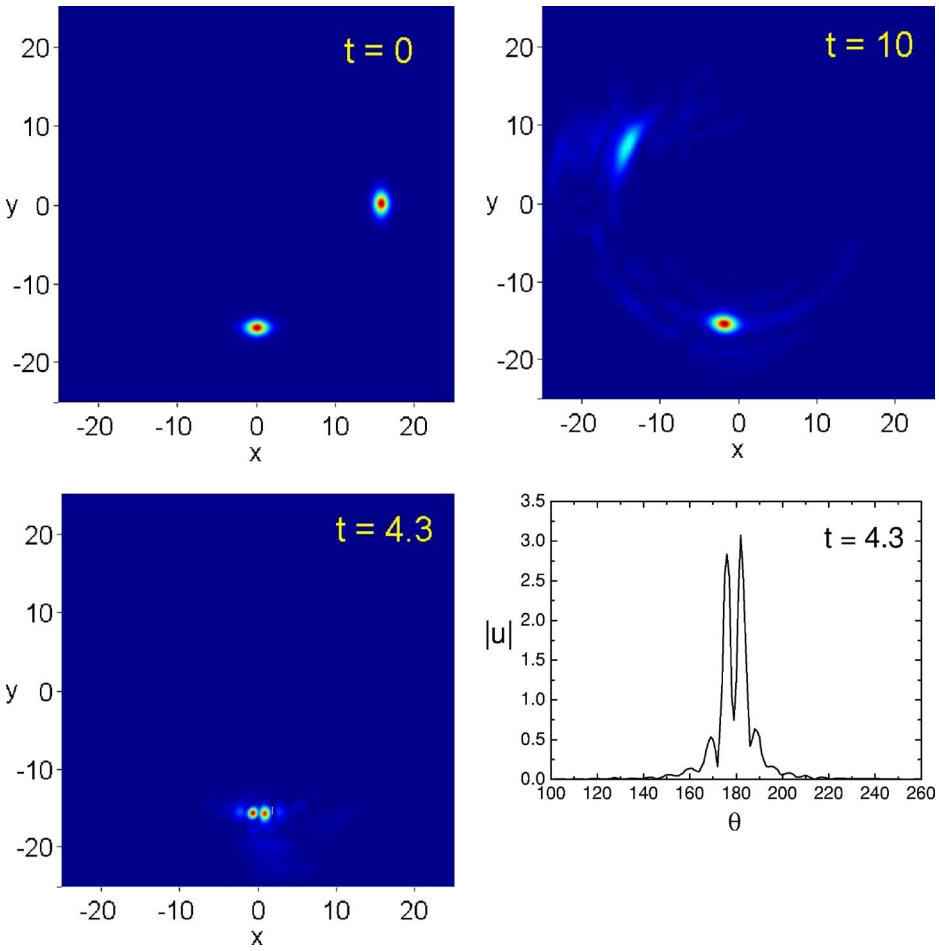

FIG. 20. (Color online) Collision between two solitons with individual norms $N=2.5\pi$ and zero phase difference, in the circular trough of radius $r_0=5\pi$. One of the solitons is set in motion (at $x=5\pi, y=0$) at $t=0$ with speed $v=3$ in the clockwise direction, while the second one (at $x=0, y=-5\pi$) stays quiescent. The norm remaining within the given circular channel at $t=10$ is $N_{\text{final}}=12.75$, i.e., 81% of the initial value. The soliton which was originally at rest loses less norm than the moving one.

sive interactions. In either case, a series of discrete eigenvalues [labeled as (a)– (d) in Fig. 8] correspond to localized states. The discrete eigenvalues are located in gaps between bands determined by the linear spectrum of Eq. (33), i.e., the respective localized solutions are the annular gap solitons which we seek for. The wave functions of the states corresponding to the discrete eigenvalues labeled in Fig. 8 are displayed in Fig. 9.

Symmetries of these localized states are similar to those of intrinsic localized modes in 1D nonlinear lattices and gap solitons in the 1D GPE with a periodic potential. Adopting the respective terminology, we will call them the onsite symmetric [Figs. 9(a) and 9(c)] and onsite antisymmetric [Figs. 9(b) and 9(d)] annular gap solitons [of course, the respective symmetry and antisymmetry are approximate ones, being violated by the curvature of the 2D model, i.e., the centrifugal potential in Eq. (33)]. Three-dimensional plots of these states are presented in Fig. 10. Notice that the antisymmetric state in the attractive model is composed of two matter-wave rings (with a phase shift of π between them) trapped in one circular trough of the potential, while its counterpart in the repulsive models feature many annular layers. The latter gap-soliton type is akin to antisymmetric "subfundamental" solitons (named so because their norm is smaller than the norm of a fundamental gap soliton found at the same value of the chemical potential), the existence of which in the second bandgap of the 1D repulsive model was reported in Ref. [40]. Actually, all the subfundamental solitons in the 1D model are unstable; the same will be demonstrated below for their counterparts in the radial model.

Stability of the annular gap solitons has been checked by direct simulations of Eq. (31). The results are reported in Fig. 11, in the $y=0$ cross section of the evolution picture. As shown in panels (a), (b), all the ring-shaped gap solitons are unstable in the attractive model, with the instability developing as the modulational instability (MI) of the originally uniform annular profile, which leads to its fragmentation into several strongly localized (spot-shaped) solitons (they are considered below). This instability is observed independently of the soliton's angular momentum.

In the repulsive model, Fig. 11(d) shows the annular gap solitons of the onsite antisymmetric type, which exist in the second bandgap [see Fig. 9(d)], are always unstable too, similar to the abovementioned "subfundamental" gap solitons in the 1D model with repulsion, which can never be stable [40]. The gap solitons of the onsite symmetric type in the repulsive model may be stable in the first bandgap, depending on their angular momentum l. The annular solitons with $l \neq 0$ are weakly unstable against azimuthal modulations of the ring's profile, as shown in Fig. 11(c). This weak instability does not lead to fragmentation of the ring, unlike the situation in the attractive model [see Fig. 11(a)]. Instead, the small azimuthal perturbation runs along the soliton's crest, thus rendering the entire structure rotating, see Fig. 11(c). This slightly disturbed rotating annular soliton persists indefinitely long. The rotation of the perturbed annular gap

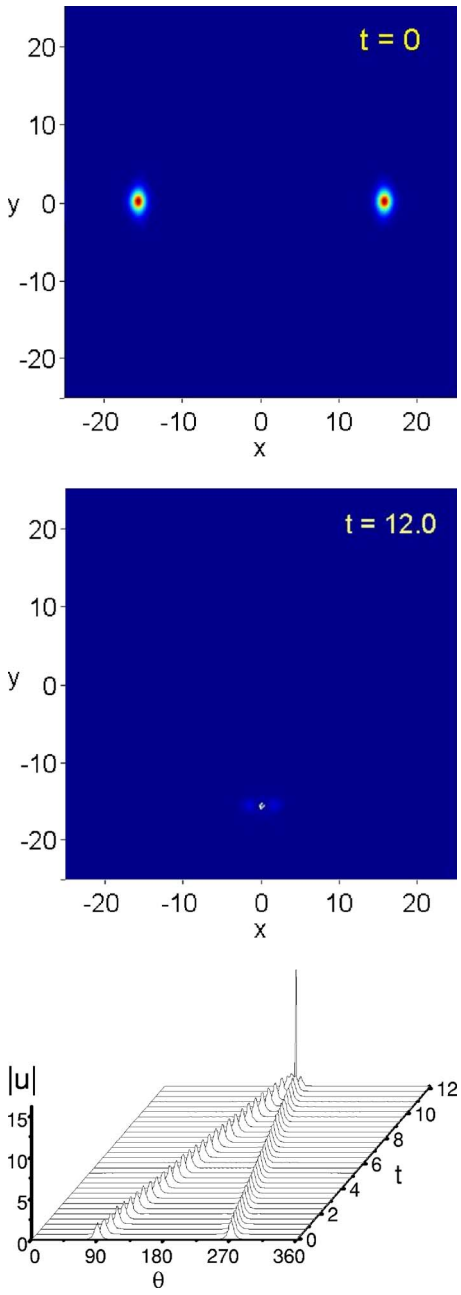

FIG. 21. (Color online) An example of collapse due to the head-on collision of two in-phase solitons in the attractive model. Both solitons were set in motion with relatively small velocities $v=\pm 1$ in one circular channel (of radius $r_0=5\pi$). Upper panels: density plots at $t=0$ and at the collapse moment ($t=12$). Lower panel: evolution of the density profiles in the cross section along the circumference of the potential trough. As in Fig. 20, the initial norm of each soliton is $N=2.5\pi$.

soliton of the latter type, and its effective stability, are additionally illustrated by means of snapshots displayed in Fig. 12.

For zero angular momentum ($l=0$), the annular gap solitons of the onsite symmetric type are completely stable in the repulsive model, as shown in Fig. 13. Other types of ring-shaped gap solitons, resembling (in the radial direction) intersite symmetric and asymmetric intrinsic localized modes

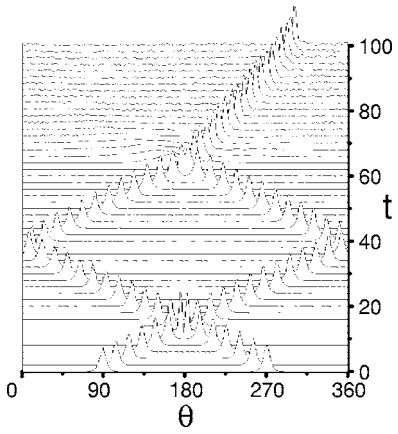

FIG. 22. Collision of two solitons for the same parameters as in Fig. 21, but with phase difference π between them. Solitons bounce at $\theta=180°$ and $\theta=0°$. Eventually, the solitons merge into a single one, avoiding collapse.

of 1D nonlinear lattices are possible too, but they turn out to be even more unstable than the onsite antisymmetric ones, in both attractive and repulsive models. In the next section, we continue the investigation of annular gap solitons of the onsite symmetric type.

VI. FURTHER NUMERICAL INVESTIGATION OF RING-SHAPED STATES

A. The repulsive model

In this section, we aim to adduce additional numerical results, which illustrate and extend general conclusions about the annular solitons and their stability made in the two preceding sections. First, it is relevant to check if gap solitons of the onsite symmetric type with $l=0$ can be found and remain stable in the repulsive model, being trapped in troughs located much farther from the center than in the examples considered above (accordingly, the soliton's norm will be much larger too), especially if the trapping potential is not as strong as above (recall that $\varepsilon=10$ in Fig. 13).

The existence and stability of the annular gap solitons in this more general case are borne out by numerical results, as illustrated by Fig. 14. This figure shows a heavy ring soliton (with $N=344.3$, cf. $N=5\pi$ in Fig. 13) of a large radius $r_0=5\pi$ (cf. $r_0=\pi$ in Fig. 13), in a relatively shallow radial potential (with $\varepsilon=3$, cf. $\varepsilon=10$ in Fig. 13). In the repulsive model, a stable ring (i.e., annual gap soliton) may additionally carry, on its crest, pairs of azimuthal dark solitons. An example of such a stable pattern is displayed in Fig. 14 (it resembles the dipole-mode ring solitons recently found in the model with repulsion and Bessel lattice in Ref. [16]). These solutions are found from simulations of Eq. (31) in real time, with absorbers set at $r=8\pi$ and $r=0$.

B. The attractive model

In Sec. IV, the MI of axisymmetric annular states in the attractive model was predicted in an analytical form. An issue of straightforward interest is an outcome of the develop-

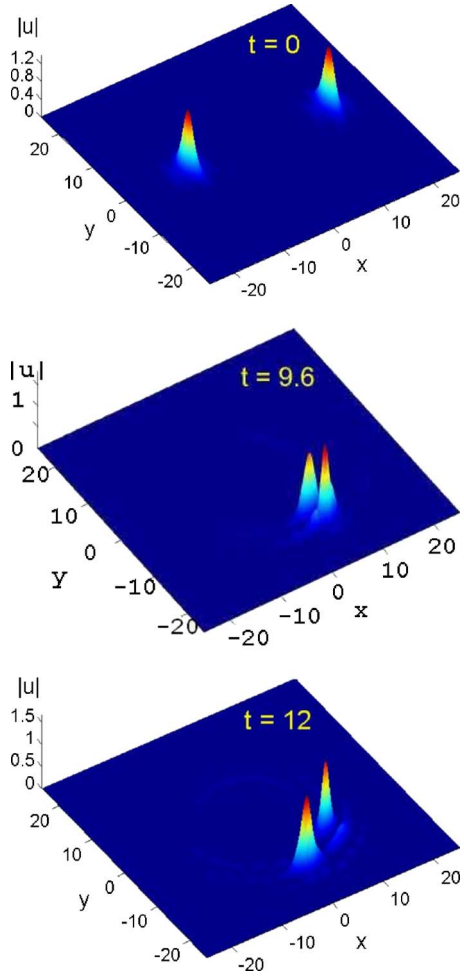

FIG. 23. (Color online) A sequence of snapshots for the collision between in-phase solitons with individual norms $N=2\pi$, moving at velocities $v=\pm 1$ in adjacent circular troughs (around $r_0=5\pi$ and $r_0=4\pi$) of the radial lattice with $\varepsilon=2$. The solitons survive the collision, and remain localized, although the collision is inelastic, giving rise to radiation loss.

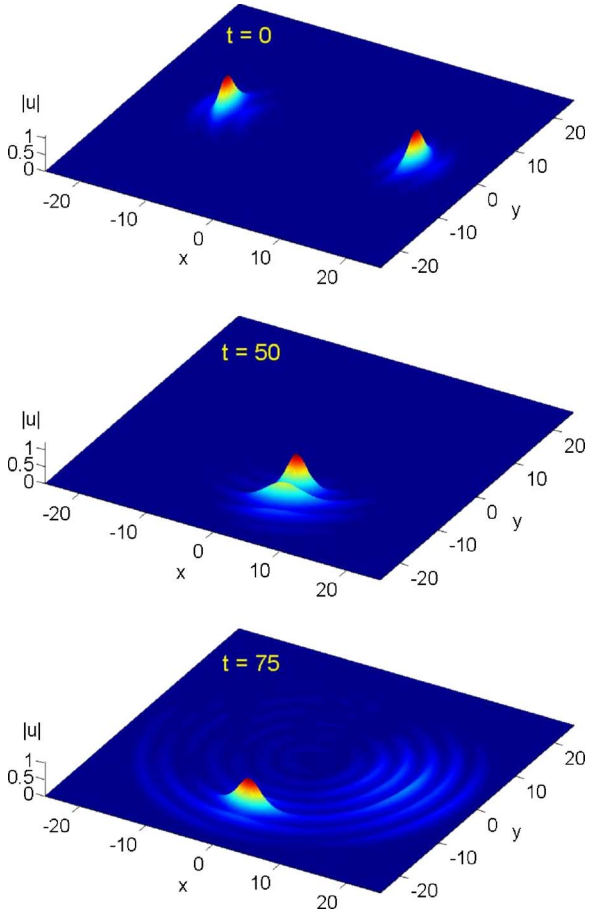

FIG. 24. (Color online) The same as in Fig. 23, but for solitons with smaller norms $N=1.7\pi$ launched to move at velocities $v=\pm 0.2$.

ment of the MI. A typical example of that is presented in Fig. 15. It is observed that the system tends to form a stationary necklacelike pattern composed of six peaks towering above the remaining quasiuniform background. Each peak may be interpreted as a strongly localized soliton.

Another typical example of a stable necklace configuration is displayed in Fig. 16, for the same radial potential as in Fig. 15 (with $\varepsilon=2$). It is generated not from an unstable axisymmetric ring, but rather from an initial set of four Gaussian pulses, with phase shifts π between them, by the integration of Eq. (1) in imaginary time.

Plausibly stable static rings with a density modulation in the azimuthal direction, corresponding to cnoidal-wave analytical solutions (21), were also predicted in the above analysis of the attractive model. Stable modulated patterns of this type were indeed found in numerical simulations, provided that the radial potential is strong enough, see an example in Fig. 17. In fact, it was generated as an outcome of the evolution of a modulationally unstable axisymmetric ring with the same norm. A transition between weakly and deeply modulated (necklacelike) stable azimuthal patterns, such as ones displayed, respectively, in Figs. 17, 15(c), and 16 occurs with the increase of the norm.

VII. ROTATIONAL DYNAMICS OF SOLITONS AND COLLISIONS BETWEEN THEM

A. Stability of rotary solitons

Strongly localized solitary waves of the attractive BEC, self-trapped in a large-radius annular potential channel, such as individual solitons in Fig. 16, can freely move in the channel (circular trough). If set in motion with a sufficiently small velocity, the soliton can circulate in the trough indefinitely long, preserving its integrity, as shown in Fig. 18.

However, if the circulation speed is too large, the centrifugal force acting on the soliton can cause the matter to tunnel into adjacent radial troughs. The loss of the norm (number of atoms) caused by the centrifugal tunneling eventually brings the soliton's norm below a threshold value necessary for its existence, which leads to disintegration of the soliton, see Fig. 19.

If the radial potential is weak, and the soliton is strongly self-trapped (with a sufficiently large norm), the centrifugal force can pull the soliton as a whole away from the

center, across the radial lattice. In that case (not shown here), the soliton also suffers the radiation loss, and eventually disintegrates.

B. Collisions between solitons

The present model offers unique possibilities for exploring interactions and collisions between matter-wave solitons, as the dynamics in circular channels is free of external perturbations, which are always present in previously reported settings (in the form of the weak longitudinal trap intended to keep the solitons within a finite spatial domain). The same advantage is offered by setups with toroidal traps [41,42]. However, sideline (tangential) collisions, which are possible between solitons moving in adjacent potential troughs of the radial lattice, have no counterparts in the latter case.

In head-on collisions of solitons in the attractive model (with both solitons trapped in one circular channel), two competing processes play major roles. The first is the nonlinear self-focusing, which may give rise to intrinsic collapse of a heavy "lump" temporarily formed by the colliding solitons, and the other is the interference due to coherence of the matter-wave solitons [10,30]. The interference pattern, featuring alternating regions of high and low density, can suppress the collapse. The predominance of either mechanism depends on the time of interaction. If it is small (i.e., the collision speed is large), solitons can pass through each other without collapse (although with conspicuous loss, see below, hence the collision cannot be termed quasielastic), even if their total norm exceeds the collapse threshold. On the contrary, slow collisions lead to the onset of collapse.

Figure 20 presents an example of a relatively fast collision between in-phase (mutually attracting) solitons. At the moment of the full overlap between them, $t=4.3$, the interference fringes are evident. They are seen too in the cross section along the circumference of the channel, in the lower right panel of Fig. 20. Although the total norm of the colliding solitons ($N_{\mathrm{tot}}=14.9$) is above the collapse threshold, and the collision time ($\Delta t \simeq 0.5$) is larger than the collapse time (which is estimated as $t_{\mathrm{collapse}} \sim 1/N_{\mathrm{tot}}$), the solitons separate without collapse. Nevertheless, the collision is essentially inelastic, the loss being additionally enhanced by the matter leakage under the action of the centrifugal force.

On the other hand, Fig. 21 shows that in-phase solitons colliding at a sufficiently small velocity merge together and eventually blow up due to the collapse. Solitons with a phase shift of π, colliding in one circular potential trough, bounce from each other due to repulsion between them. Then, repeated bouncing collisions are observed, which is similar to the dynamics in the Bessel lattice [14], as well as in a quasi-1D OL, supplemented by a weak longitudinal trap [10]. However, in contrast to those cases, we have observed that many collisions in the circular trough gradually wash out the phase coherence between the solitons. As a result, the solitons cease to repel each other, and a clear interference pattern disappears. Eventually, the originally repelling solitons merge together, shedding the excessive norm away, as shown in Fig. 22. The collapse does not occur in this case, as the loss pushes the norm of the finally established single soliton below the collapse threshold.

The present setting makes it also possible to investigate tangential collisions between solitons moving in adjacent channels of the radial potential. The result is that two in-phase solitons tend to merge, due to the flow of matter between them (a similar trend was observed in Ref. [10], in simulations of tangential collisions in the 2D model with a quasi-1D lattice). Nevertheless, the solitons may avoid the merger and separate, if the collision time is small due to a large relative velocity, as shown in Fig. 23.

On the other hand, if each soliton is a loosely bound one (i.e., its norm is small and/or the radial lattice is weak), slow lateral collisions give rise to merger of the solitons into one. Collapse is avoided in this case, due to shedding off excessive norm with linear waves, as demonstrated in Fig. 24.

VIII. CONCLUSIONS

In this work, we have proposed a new setting to explore two-dimensional (2D) localized states in self-attractive and repulsive BECs, in the form of a periodic radial optical lattice. A crucial difference from previously studied 2D models with Bessel lattices is the fact that the linear limit of the present model supports no localized states, hence all localized states in it are "true solitons," impossible without the nonlinearity. In addition to the BEC, the model may also apply to spatial solitons (beams) in photonic crystal fibers with a circular intrinsic structure.

The existence of solitons in this setting was demonstrated by means of different variants of the variational approximation, and in direct numerical simulations. We have investigated two distinct classes of localized states existing in the model, viz., ones trapped in the central potential well, and in remote circular potential troughs. In each class, a new soliton species, namely, stable radial gap solitons, has been identified in the model with self-repulsion (in addition, the radial gap soliton trapped in a circular trough can carry stable pairs of azimuthal dark solitons on its crest). The solitons trapped in the central potential well are stable, in the case of attraction and repulsion alike.

Annular gap solitons in the repulsive model, trapped in circular potential troughs far from the center, are completely stable if they carry zero angular momentum, $l=0$. The same solitons with $l \neq 0$ develop a small-amplitude azimuthal modulation, and persist indefinitely long in the form of rotating weakly modulated ring patterns.

In the attractive model, we have investigated ring-shaped patterns delocalized in the azimuthal direction, and strongly localized azimuthal solitons (including moving ones), both trapped in a remote potential circular trough. Solutions of these types are described by an effective 1D equation supplemented by periodic boundary conditions (it is a nonpolynomial NLS equation with the coordinate running along the circumference). Using that equation, a threshold of the azimuthal modulational instability (MI) of axisymmetric ring-shaped states was predicted, and exact cnoidal-wave solutions, generated by the MI-induced bifurcation just above the MI threshold, were found. Azimuthal solitons were also found as solutions of the same equation. The existence of stable weakly modulated ring-shaped states was corroborated

by direct simulations. In a more general case, the development of the MI leads to the establishment of stable necklace patterns, composed of several (for instance, four or six) strongly localized peaks.

Dynamics of completely localized solitons in the attractive model circulating in the annular potential troughs was investigated too. The solitons with sufficiently small velocities remain stable indefinitely long, while high velocities give rise to leakage of matter into the adjacent (more remote) trough under the action of the centrifugal force, which eventually destroys the soliton. We have also investigated collisions between solitary waves running in the same or adjacent circular channels. Head-on collisions of in-phase solitons in one trough lead to collapse; π-out of phase solitons bounce from each other many times, but gradually lose the mutual coherence, and eventually merge into a single soliton, avoiding collapse by shedding the overcritical norm. In-phase solitons colliding in adjacent channels may also merge into a single soliton.

ACKNOWLEDGMENTS

B.B.B. is partially supported by Grant No. 20-06 from the Fund for Fundamental Research of the Uzbek Academy of Sciences. The work of B.A.M. was supported, in part, by the Israel Science Foundation through the Center-of-Excellence Grant No. 8006/03. M.S. acknowledges financial support from MIUR, through the inter-university project, "Dynamical properties of Bose-Einstein condensates in optical lattices," Grant No. PRIN-2005.

[1] J. Denschlag, J. E. Simsarian, D. L. Feder, C. W. Clark, L. A. Collins, J. Cubizolles, L. Deng, E. W. Hagley, K. Helmerson, W. P. Reinhardt, S. L. Rolston, B. I. Schneider, and W. D. Phillips, Science **287**, 97 (2000); S. Burger, K. Bongs, S. Dettmer, W. Ertmer, K. Sengstock, A. Sanpera, G. V. Shlyapnikov, and M. Lewenstein, Phys. Rev. Lett. **83**, 5198 (1999).

[2] L. Khaykovich, F. Schreck, G. Ferrari, T. Bourdel, J. Cubizolles, L. D. Carr, Y. Castin, and C. Salomon, Science **296**, 1290 (2002).

[3] K. E. Strecker, G. B. Partridge, A. G. Truscott, and R. G. Hulet, Nature (London) **417**, 150 (2002).

[4] S. L. Cornish, S. T. Thompson, and C. E. Wieman, Phys. Rev. Lett. **96**, 170401 (2006).

[5] N. G. Parker, A. M. Martin, S. L. Cornish, and C. S. Adams, cond-mat/0603059.

[6] L. Khaykovich and B. A. Malomed, Phys. Rev. A **74**, 023607 (2006).

[7] B. Eiermann, Th. Anker, M. Albiez, M. Taglieber, P. Treutlein, K.-P. Marzlin, and M. K. Oberthaler, Phys. Rev. Lett. **92**, 230401 (2004).

[8] V. A. Brazhnyi and V. V. Konotop, Mod. Phys. Lett. B **18**, 627 (2004); O. Morsch and M. Oberthaler, Rev. Mod. Phys. **78**, 179 (2006).

[9] B. A. Malomed, D. Mihalache, F. Wise, and L. Torner, J. Opt. B: Quantum Semiclassical Opt. **7**, R53 (2005).

[10] B. B. Baizakov, B. A. Malomed, and M. Salerno, Phys. Rev. A **70**, 053613 (2004).

[11] D. Mihalache, D. Mazilu, F. Lederer, Y. V. Kartashov, L.-C. Crasovan, and L. Torner, Phys. Rev. E **70**, 055603(R) (2004).

[12] M. Trippenbach, M. Matuszewski, and B. A. Malomed, Europhys. Lett. **70**, 8 (2005); M. Matuszewski, E. Infeld, B. A. Malomed, and M. Trippenbach, Phys. Rev. Lett. **95**, 050403 (2005).

[13] B. A. Malomed, *Soliton Management in Periodic Systems* (Springer, New York, 2006).

[14] Y. V. Kartashov, V. A. Vysloukh, and L. Torner, Phys. Rev. Lett. **93**, 093904 (2004).

[15] Y. V. Kartashov, V. A. Vysloukh, and L. Torner, Phys. Rev. Lett. **94**, 043902 (2005).

[16] Y. V. Kartashov, R. Carretero-Gonzalez, B. A. Malomed, V. A. Vysloukh, and L. Torner, Opt. Express **13**, 10703 (2005).

[17] N. Moiseyev, L. D. Carr, B. A. Malomed, and Y. B. Band, J. Phys. B **37**, L193 (2004).

[18] L. D. Carr, M. J. Holland, and B. A. Malomed, J. Phys. B **38**, 3217 (2005).

[19] Q. E. Hoq, P. G. Kevrekidis, D. J. Frantzeskakis, and B. A. Malomed, Phys. Lett. A **341**, 145 (2005).

[20] X. Wang, Z. Chen, and P. G. Kevrekidis, Phys. Rev. Lett. **96**, 083904 (2006).

[21] D. Mihalache, D. Mazilu, F. Lederer, B. A. Malomed, Y. V. Kartashov, L.-C. Crasovan, and L. Torner, Phys. Rev. Lett. **95**, 023902 (2005).

[22] A. S. Desyatnikov, A. A. Sukhorukov, and Y. S. Kivshar, Phys. Rev. Lett. **95**, 203904 (2005).

[23] E. Lidorikis, M. Soljaćić, M. Ibanescu, Y. Fink, and J. D. Joannopoulos, Opt. Lett. **29**, 851 (2004).

[24] Z. H. Musslimani and J. Yang, J. Opt. Soc. Am. B **21**, 973 (2004); M. J. Ablowitz and Z. H. Musslimani, Opt. Lett. **30**, 2140 (2005).

[25] M. L. Chiofalo, S. Succi, and M. P. Tosi, Phys. Rev. E **62**, 7438 (2000).

[26] J. Durnin, J. J. Miceli, and J. H. Eberly, Phys. Rev. Lett. **58**, 1499 (1987).

[27] A. Görlitz, J. M. Vogels, A. E. Leanhardt, C. Raman, T. L. Gustavson, J. R. Abo-Shaeer, A. P. Chikkatur, S. Gupta, S. Inouye, T. Rosenband, and W. Ketterle, Phys. Rev. Lett. **87**, 130402 (2001).

[28] B. B. Baizakov, V. V. Konotop, and M. Salerno, J. Phys. B **35**, 5105 (2002); E. A. Ostrovskaya and Y. S. Kivshar, Phys. Rev. Lett. **90**, 160407 (2003).

[29] B. B. Baizakov, B. A. Malomed, and M. Salerno, Europhys. Lett. **63**, 642 (2003).

[30] B. B. Baizakov, M. Salerno, and B. A. Malomed, in *Nonlinear Waves: Classical and Quantum Aspects*, edited by F. Kh. Abdullaev and V. V. Konotop (Kluwer Academic, Dordrecht, 2004), p. 61; also available at http://rsphy2.anu.edu.au/~asd124/Baizakov_2004_61_Nonlinear Waves.pdf

[31] M. G. Vakhitov and A. A. Kolokolov, Radiophys. Quantum Electron. **16**, 783 (1973).

[32] L. Bergé, Phys. Rep. **303**, 260 (1998).

[33] B. A. Malomed, Prog. Opt. **43**, 69 (2002).
[34] M. Desaix, D. Anderson, and M. Lisak, J. Opt. Soc. Am. B **8**, 2082 (1991).
[35] B. A. Malomed, Z. H. Wang, P. L. Chu, and G. D. Peng, J. Opt. Soc. Am. B **16**, 1197 (1999).
[36] L. Stenflo and O. M. Gradov, IEEE Trans. Plasma Sci. **PS-14**, 554 (1986); L. Stenflo, J. Phys. A **21**, L499 (1988).
[37] L. D. Carr, C. W. Clark, and W. P. Reinhardt, Phys. Rev. A **62**, 063610 (2000).
[38] L. D. Carr, C. W. Clark, and W. P. Reinhardt, Phys. Rev. A **62**, 063611 (2000).
[39] M. Salerno, Laser Phys. **15**, 620 (2005).
[40] T. Mayteevarunyoo and B. A. Malomed, Phys. Rev. A **74**, 033616 (2006).
[41] S. Gupta, K. W. Murch, K. L. Moore, T. P. Purdy, and D. M. Stamper-Kurn, Phys. Rev. Lett. **95**, 143201 (2005).
[42] A. Parola, L. Salasnich, R. Rota, and L. Reatto, Phys. Rev. A **72**, 063612 (2005); R. Kanamoto, H. Saito, and M. Ueda, *ibid.* **73**, 033611 (2006).